SH wave propagation in joined half-spaces composed of elastic metamaterials

Xiaona Shi, Haisheng Shu (ID), Haiyong Zhou, Lei Zhao, Ru Liu, Shuowei An, and Jie Zhu

View Online   **Export Citation**   **CrossMark**

ARTICLES YOU MAY BE INTERESTED IN

SH wave propagation in joined half-spaces composed of elastic metamaterials

Xiaona Shi,[1] Haisheng Shu,[1,2,a)] Haiyong Zhou,[3] Lei Zhao,[1] Ru Liu,[1] Shuowei An,[1] and Jie Zhu[2,a)]

[1]*Mechanical and Electrical Engineering College, Harbin Engineering University, 150001 Harbin, China*
[2]*Department of Mechanical Engineering, The Hong Kong Polytechnic University, Hung Hom, Kowloon, Hong Kong, China*
[3]*Shanghai Marine Equipment Research Institute, China Shipbuilding Industry Corporation (CSIC), Shanghai 200031, China*

Based on the effective-medium theory, the propagation of a shear horizontal (SH) wave in joined half-spaces composed of elastic metamaterials (EMMs) is investigated. From the dispersion relations, the effects of negative effective-medium parameters on the properties of a SH wave traveling near the interface are analyzed in detail. It is found that a SH wave can always appear and travel along the interface under specific effective-parameter combinations no matter whether the effective transverse wave velocity is imaginary or real. This is significantly different from the classical case (joined half-spaces composed of natural media), and the existence of these SH interfacial wave modes may have important impacts on EMM-based SH wave manipulation, especially wave isolation and object protection. *Published by AIP Publishing.* https://doi.org/10.1063/1.4994611

I. INTRODUCTION

Originating from the work of Liu *et al.*[1] in 2000, an elastic metamaterial (EMM) is a new type of composite that is composed of many sub-wavelength unit cells embedded in a certain matrix. Unlike the case of phononic crystals (Bragg type), whose periodicity is the decisive factor, the special wave properties of EMMs are attributed mainly to the unique properties of the internal sub-wavelength unit cell that create differing resonant behaviors. By using an EMM, elastic waves can be manipulated in unprecedented ways, for example, the isolation of elastic waves within low and medium frequency,[2–5] elastic-wave cloaking,[6,7] negative refraction,[8–10] energy localization,[11,12] and super-resolution imaging.[13] This field is very active nowadays, and more information can be found in Refs. 14 and 15.

Existing studies have shown that the behavior of waves in an EMM can be described effectively using the concept of an effective medium and homogenization technology under long-wave conditions [i.e., the internal unit cell (scatterer) is much smaller than the wavelength in the matrix]. The effective-medium parameters of an EMM are generally frequency-dependent and can become negative near the vibrational eigenmodes of the scatterer.[5,16–18] Moreover, it has been recognized that the negative effective bulk modulus, effective density, and effective shear modulus are associated with the monopole, dipole, and quadrupole resonant modes, respectively, of the scatterer.[18–21] In fact, the band gaps and negative-refraction properties of EMMs are related directly to these negative effective parameters; for instance, single-negative effective parameters often lead to the band gaps of bulk waves,[3,22] and double-negative or triple-negative effective parameters can induce negative refraction.[23,24] Based on this understanding, a variety of subtle sub-wavelength unit cells have been proposed from which EMMs can be constructed[21,25–29] to achieve certain functions of wave control. The frequency-dependent effective parameters can be evaluated using the effective-medium theory, for which the Coherent Potential Approximation (CPA) method[20,30,31] and the "feel and response" method[32–35] are frequently used. EMMs with different negative effective parameters (i.e., single-, double-, and triple-negativities) have been realized recently.[3,19,21,36,37] In addition, wave reflection and transmission occurring at the interface of two different EMMs have also been investigated,[23] through which unique phenomena such as negative refraction and wave-mode conversion have been revealed. Given that natural materials do not present these effective parameters, EMM-based designs have also been proposed for isolating certain important elastic waves, especially seismic waves.[38–41]

As for practical problems, there always exist different surface or interface boundaries. The classical wave theory[42,43] supports certain types of surface or interfacial waves (IWs), such as the well-known Rayleigh, Stoneley, and Love waves. When it comes to EMMs instead of natural media, it is not difficult to imagine that similar surface/IWs could also exist under certain conditions because an EMM can be deemed an extension of a natural medium from the effective-medium perspective. Although related studies on surface or interfacial wave propagation in EMMs are relatively few, a surface wave akin to a surface plasmon polariton (SPP)[44] has been found recently on the surface of an EMM with specific effective parameters, and the conditions for Rayleigh and Scholte waves to exist in an EMM were established and verified by finite-element simulations. Although these surface or interfacial waves are obviously detrimental in EMM-based elastic-wave isolation applications and should be attended to carefully, they could be useful in certain function devices of elastic (acoustic) waves.

a)Authors to whom correspondence should be addressed: shujs@hrbeu.edu.cn and jie.zhu@polyu.edu.hk

In the present paper, we derive the dispersion relation of a shear horizontal (SH) wave propagating in joined half-spaces composed of one or more EMMs. We also analyze in detail the effects of negative effective-medium parameters on the ability of the SH wave to travel near the interface, as well as its properties in doing so. We find that no matter whether the effective transverse wave velocity is imaginary or real, a class of SH traveling waves can always appear near the interface when certain existence conditions (four specific combinations of effective parameters) are satisfied. This observation clearly differs from the classic case (i.e., joined half-spaces composed of natural media), and the existence of these SH IW modes may significantly impact EMM-based SH wave isolation and object protection.

This paper is organized as follows: an analytical model of joined half-spaces composed of one or more EMMs is given in Sec. II, and the dispersion relation of a SH IW is deduced. According to different combinations (positive or negative) of effective-medium parameters, the conditions for a SH IW mode to exist are discussed further, and in Sec. III, we establish four supporting conditions involving the effective density and/or the shear modulus ratio between the two half-spaces. The theoretical results given in Sec. III are verified in Sec. IV by finite-element simulations at two levels, namely, that of the effective medium and that of the microstructural unit cell. Finally, conclusions and potential future work are given in Sec. V.

II. MODEL AND DISPERSION EQUATIONS

Although a SH wave propagating in joined half-spaces is a classic problem, we are concerned mainly here with a SH IW mode traveling near the interface. It is well known that when both sides of the joined half-spaces are composed of normal media, no surface wave mode can exist according to the classical wave theory.[43] However, the situation is very different when one or more EMMs are used to construct the joined half-spaces.

As shown in Fig. 1, the upper and lower half-spaces are assumed to be composed of an EMM medium and a normal one, respectively. It is worth noting that both the effective density and effective shear modulus of an EMM can be designed to be frequency-dependent, which has additional impacts on the dispersion relation of a SH wave in joined half-spaces. Actually, 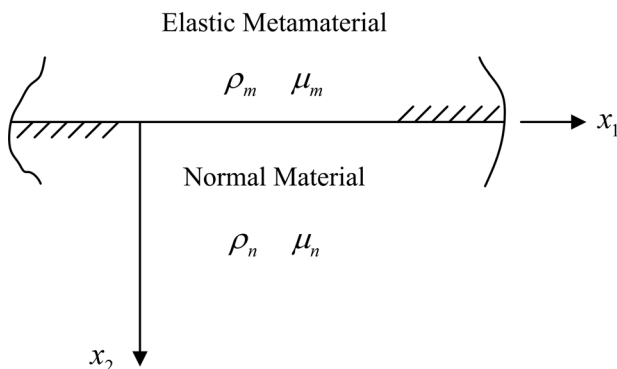the analysis is similar to that of the general case. This is because their effects on the SH wave properties are exhibited directly through the effective transverse wave velocity. The frequency-dependent effective density used here is a very typical one that is borrowed from Ref. 27 [see Eq. (14) therein]; the frequency response function (FRF) curve is shown in Fig. 2, where ω_0 is the characteristic frequency of the built-in unit of the EMM (see the inset), and ρ_m and ρ_{st} represent the effective and static densities, respectively. On the whole, the frequency response of the effective density can be regarded as a type of resonance curve. The effective density increases gradually from its static value to infinity when approaching the critical frequency ω_0 from below, it becomes negative when beyond ω_0, and it then tends to zero gradually in a certain frequency band with further increase of frequency. The effective density ρ_m and shear modulus μ_m of the EMM can become negative within certain frequency regions.

The displacement solutions of a SH wave in the two media can be expressed as

$$u_3^m = C_1 e^{jpx_2} e^{j(kx_1-\omega t)},$$
$$u_3^n = C_2 e^{jqx_2} e^{j(kx_1-\omega t)}, \quad (1)$$

where $p^2 = \frac{\omega^2}{c_m^2} - k^2$, $c_m^2 = \frac{\mu_m}{\rho_m}$, $q^2 = \frac{\omega^2}{c_0^2} - k^2$, and $c_0^2 = \frac{\mu_n}{\rho_n}$. Terms p and q are the wavenumbers of the upper and lower half-spaces in the x_2 direction, respectively. The term k is the wavenumber in the x_1 direction, and j is the imaginary unit. The density ρ_n and shear modulus μ_n of the normal medium are positive constants.

To meet the continuity conditions of displacement and shearing stress on the interface, we have the following relations:

$$C_1 = C_2, \quad (2)$$

$$\mu_m p = \mu_n q. \quad (3)$$

We are concerned here with a surface wave traveling in the ρ_m, μ_m direction near the interface, so p and q should take negative and positive imaginary values, respectively. Hence, $k^2 > \frac{\omega^2}{c_m^2}$ and $k^2 > \frac{\omega^2}{c_0^2}$ must be satisfied as prerequisites. Let $p = jp^*$, $p^* = -\sqrt{k^2 - \frac{\omega^2}{c_m^2}}$, $q = jq^*$, and $q^* = \sqrt{k^2 - \frac{\omega^2}{c_0^2}}$, whereupon Eq. (3) can be expanded as
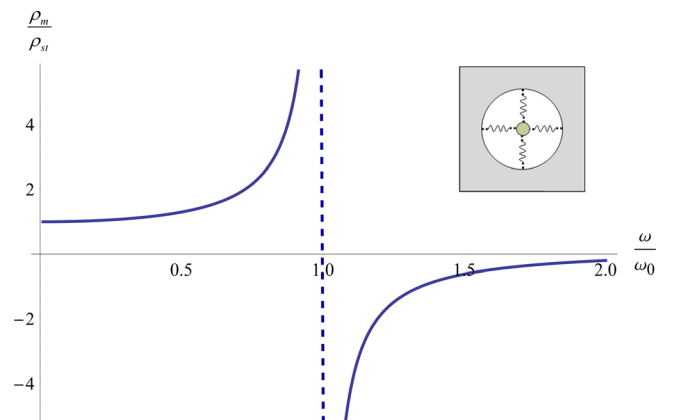

FIG. 1. Joined half-spaces built from an elastic metamaterial (EMM) and a normal material.

FIG. 2. Frequency response function (FRF) of the typical effective density.

$$\frac{-\sqrt{k^2 - \dfrac{\omega^2}{c_m^2}}}{\sqrt{k^2 - \dfrac{\omega^2}{c_0^2}}} = \frac{\mu_n}{\mu_m}. \tag{4}$$

Equations (3) or (4) give the dispersion relation that should be satisfied by an IW traveling in the joined half-spaces. Unlike the normal case (i.e., joined half-spaces composed of two normal media) in which the relation never holds, the dispersion relation may be met under certain conditions by engineering the effective shear modulus (μ_m) of the EMM half-space to be negative within certain frequency regions. In the following, different cases are discussed according to the characteristics of the effective parameters of the EMM.

III. DISCUSSION OF SH IW MODES

A. Joined half-spaces composed of an EMM and a normal material

If the lower half-space is composed of a normal medium, there are four different combinations according to whether the effective parameters of the EMM half-space are positive or negative.

(1) Double-positive parameters ($\rho_m > 0$, $\mu_m > 0$)

When $\rho_m > 0$ and $\mu_m > 0$, the left-hand-side of Eq. (4) is negative whereas the right-hand side is positive. Hence, the dispersion relation can never be met, meaning that no SH IW mode can appear and travel in the joined half-spaces under these conditions. It is noted that there exists a limiting case of $p = q = 0$, which requires $c_m^2 = c_0^2$; obviously, Eq. (3) holds in that case and we have $c_m = c_0 = \frac{\omega}{k}$. However, as seen from the displacement solution [Eq. (1)], the displacement fields of the upper and lower half-spaces become independent of $\frac{\omega}{\omega_0}$, which actually represent a class of bulk SH waves propagating in the $b \rightarrow a$ direction as a whole.

Thus, we conclude that there is no SH IW mode that can travel in the vicinity of the interface formed by a normal half-space and an EMM one with double-positive effective parameters. Undoubtedly, this point is also applicable to joined half-spaces that are both composed of normal media.

(2) Single-negative effective density ($\rho_m < 0$, $\mu_m > 0$)

As in the previous case, Eq. (4) also cannot be met with $\rho_m < 0$ and $\mu_m > 0$, and so no SH IW mode exists. Somewhat differently, the situation of $p = q = 0$ does not appear here because $c_m^2 < 0$ while $c_0^2 > 0$ (the limiting case of both being zero represents both half-spaces being composed of fluid-like media and hence no SH wave arises).

Consequently, there is also no SH mode at the interface formed by a normal half-space and an EMM one with single-negative effective density.

(3) Single-negative effective shear modulus ($\rho_m > 0$, $\mu_m < 0$)

If $\rho_m > 0$ and $\mu_m < 0$, both sides of Eq. (4) are less than zero simultaneously. Therefore, certain solutions may exist. For convenience, two ratios of medium parameters are introduced here, namely, $a = \frac{\rho_m}{\rho_n}$ and $b = \frac{-\mu_m}{\mu_n}$ ($a > 0, b > 0$). Then, according to Eq. (4), we obtain $k = \sqrt{\frac{1+ab}{1-b^2}}\frac{\omega}{c_0}$. Apparently, a traveling IW mode does exist (with real wavenumber k) as long as the condition $0 < b < 1$ is satisfied.

A set of parameters ($b = 0.2$, 0.8, 0.94, 0.97, 0.99, and 0.999, $\rho_n = 2600 \text{ kg/m}^3$, and $\mu_n = 9 \text{ MPa}$) is chosen for numerical calculation. Meanwhile, the typical frequency-dependent effective density is also considered here, which is similar to that given in Sec. II except that the vertical coordinate is replaced by a in Fig. 2 and the characteristic frequency ω_0 is set as 600 rad/s. It should be noted that these parameter values are selected arbitrarily here and do not correspond to a specific natural medium. In fact, it can be seen that the ratios of density and shear modulus (i.e., a and b, respectively) are the decisive factors in the dispersion relation ($k = \sqrt{\frac{1+ab}{1-b^2}}\frac{\omega}{c_0}$) and hence specific values of parameters such as density and shear modulus have no radical influences on the main conclusions. The dispersion curves as calculated are depicted in Fig. 3, where the horizontal axis (k) represents the wavenumber in the x_1 direction and the vertical axis denotes the dimensionless frequency.

First, it can be observed that all the curves of SH IW modes are located below and to the right of the bulk transverse wave mode of the normal half-space, i.e., the black dashed line ($\omega = kc_0$) shown in Fig. 3. In fact, it is noted that the prerequisite $k^2 > \frac{\omega^2}{c_0^2}$ holds only within this region, which is essential to ensure that q is imaginary (an imaginary value of p is ensured by $c_m^2 < 0$).

Second, the dispersion curves are gradually approaching the straight line $\omega = kc_0$ as the shear modulus ratio b tends
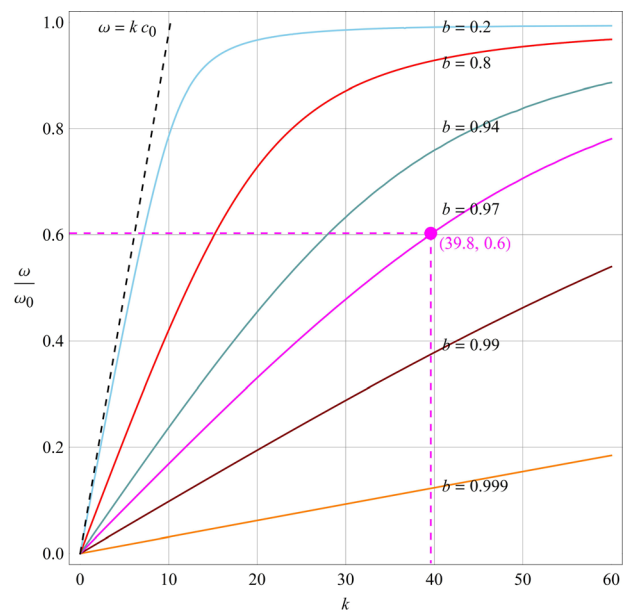

FIG. 3. Dispersion curves of SH interfacial wave (IW) modes traveling in joined half-spaces composed of a normal medium and an EMM one with a typical effective density ($\omega_0 = 600$ rad/s) and different ratios of shear moduli ($b = 0.2$, 0.8, 0.94, 0.97, 0.99, and 0.999).

to zero (or equivalently as $\mu_m \to 0$). In other words, the SH IW velocity will tend to the bulk transverse wave velocity of the normal-medium half-space. In fact, as b tends to zero, the SH wave can hardly be transferred effectively in the EMM half-space because the EMM becomes ever-more fluid-like. Meanwhile, the boundary surface (or the interface) of the normal half-space becomes gradually similar to a stress-free boundary in terms of the SH wave motion. It should be noted that the wavenumber q^* in the x_2 direction is also approaching zero as b tends to zero. Hence, the displacement solution [the second one of Eq. (1)] will tend to represent a bulk SH wave in the lower half-space as a whole in the x_1 direction, which is denoted by the black dashed line $\omega = kc_0$. Consequently, the SH IW velocity should approach the value of c_0 as b tends to zero, as observed from Fig. 3.

Third, the wavenumber k (in the x_1 direction) of the IW will increase gradually for a given frequency as b tends to unity, and meanwhile, the wave amplitude attenuation becomes ever stronger along the x_2 direction (refer to the expressions for p^* and q^*). Therefore, the IW will travel along the x_1 direction with the displacement field confined to an ever-narrower region on either side of the interface as b approaches unity. We note in passing that the resultant wavenumbers in the EMM and normal half-spaces remain always unchanged as ω/c_m and ω/c_0, respectively. The limiting case of $b = 1$ is considered additionally; the continuity condition of shearing stress on the interface can no longer be satisfied physically, as can easily be observed from Eq. (3). Besides, looking at the displacement solutions, we find that the displacement field will vanish completely on either side and exist exactly on the interface formed by the two half-spaces under this limiting case, which is apparently nonphysical but nevertheless a mathematical (albeit limiting) solution (i.e., $k = \infty$).

Finally, we consider the IW behavior as ω tends to ω_0. As the effective density gradually approaches infinity (or equivalently as $a \to \infty$), all of the dispersion curves tend to be horizontal and approach the common asymptotic line

$\omega = \omega_0$. In fact, this reflects the fact that the hypothetical particles of the effective medium of the EMM could hardly be stimulated to vibrate because their individual mass would become much greater as ω tends to ω_0. Correspondingly, the vibration energy could hardly be transferred in the form of wave motion, and hence, the group velocity would tend to zero and the dispersion curves would approach the horizontal asymptote at $\omega = \omega_0$.

(4) Double-negative parameters ($\rho_m < 0$, $\mu_m < 0$)

The solution of Eq. (4) in this case is analogous to that in the previous one. Introducing $a = \frac{-\rho_m}{\rho_n}$ and $b = \frac{-\mu_m}{\mu_n}$ ($a > 0, b > 0$), the dispersion relation of the SH IW can be obtained from Eq. (4) as $k = \sqrt{\frac{1-ab}{1-b^2}}\frac{\omega}{c_0}$. Considering the prerequisites of $k^2 > \frac{\omega^2}{c_m^2}$ and $k^2 > \frac{\omega^2}{c_0^2}$, $\sqrt{\frac{1-ab}{1-b^2}} > 1$ and $\sqrt{\frac{1-ab}{1-b^2}}\sqrt{\frac{b}{a}} > 1$ must be satisfied simultaneously. Consequently, the following two supporting conditions for the SH IW mode can be derived in this case:

$$\text{Condition A1}: 0 < a < b < 1 \quad \text{and}$$

$$\text{Condition A2}: 1 < b < a.$$

These manifest the fact that an IW could exist and travel in joined half-spaces composed of a normal medium and an EMM with double-negative effective parameters as long as the ratios of effective density and effective shear modulus meet specific supporting conditions. For illustration, we choose two sets of parameters satisfying the above two conditions respectively ($a = 0.45$, $b = 0.5$, 0.9, 0.97, 0.99, and 0.999; $a = 3$, $b = 1.002$, 1.03, 1.1, 1.3, and 2.5) are chosen to calculate the dispersion curves of the IW. The results are shown in Fig. 4.

For the case in which the effective parameter ratios satisfy condition A1, the dispersion curves are shown in Fig. 4(a). It can be seen that as b tends to a, the IW mode tends to the bulk transverse wave mode of the normal half-space, which is represented by the black dashed line $\omega = kc_0$. In
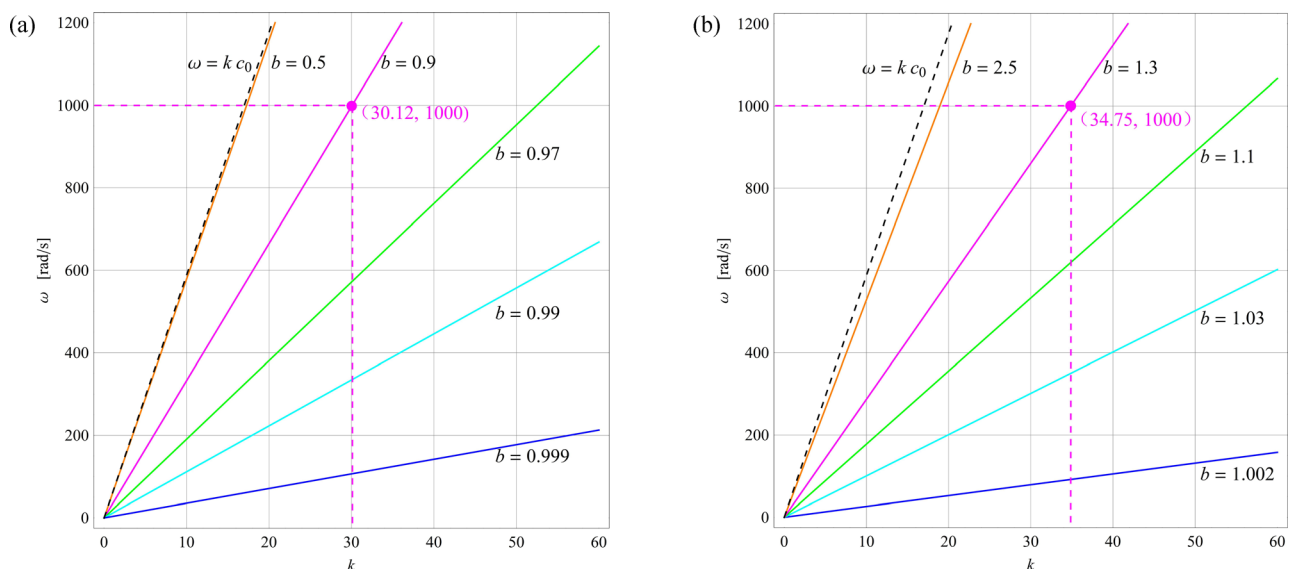

FIG. 4. Dispersion curves of the SH IW mode in joined half-spaces composed of a normal-medium half-space and an EMM half-space with double-negative effective parameters. (a) $a = 0.45$, $b = 0.5$, 0.9, 0.97, 0.99, 0.999 and (b) $a = 3$, $b = 1.002$, 1.03, 1.1, 1.3, 2.5.

fact, as b tends to a, the transverse wave velocities in the upper and lower half-spaces tend to the same value (i.e., $c_m \rightarrow c_0$) according to the definition of bulk transverse wave velocity. Consequently, $p = \sqrt{\frac{\omega^2}{c_m^2} - k^2}$ and $q = \sqrt{\frac{\omega^2}{c_0^2} - k^2}$ will also tend to be equal. To meet the continuity requirement [Eq. (3)] of shearing stress on the interface, it can be found that p and q should approach zero simultaneously. As can be seen clearly from Eq. (1), this represents simply a kind of SH wave for both the upper and lower half-spaces in the x_1 direction, i.e., the bulk transverse wave mode ($\omega = kc_0$). Similar to the previous case, the interfacial wavenumber k also increases gradually for a given frequency as b tends to unity, and the wave field tends to be confined to an ever-narrower region on either side of the interface. In addition, there exists a limiting case, namely, $b = a = 1$, in which the effective density and effective shear modulus of the EMM half-space are exactly opposite to those of the lower normal half-space, seemingly like a type of "antimatter." By checking Eq. (3) or (4), we see that the continuity condition of shearing stress on the interface (or the dispersion relation) can always be satisfied, meaning that an IW mode with an arbitrary real wavenumber k can appear at any frequency in this limiting case. Nevertheless, it should be noted that the resultant wavenumbers of these IW modes in both half-spaces remain unchanged and keep the same value, namely $\frac{\omega}{c_0}$ (or $\frac{\omega}{c_m}$, because $c_m = c_0$ here).

For the other case in which the effective parameter ratios satisfy condition A2, the dispersion curves are depicted in Fig. 4(b). The results are similar: the IW velocity will approach the bulk transverse wave velocity of the normal half-space as b tends to a, while its wavenumber will gradually increase and tend to infinity as b tends to unity.

In passing, it can be seen that the effective parameters (effective density and shear modulus) in the above case of double-negative parameters are assumed to be independent of the wave frequency to simplify the analysis and focus on the essential factors. In fact, the frequency dependence of these effective parameters cannot fundamentally affect the results obtained here because whether the SH IW exists or not is determined mainly by the negative properties of these effective parameters. Certainly, within the frequency range corresponding to double-negative parameters, the frequency dependencies of these effective parameters do influence the location of the frequency band in which the IW appears through influencing the values of a and b, i.e., the effective parameter ratios. However, it is impossible for us to study all possible types of frequency dependency of the effective parameters, therefore, the simplification here is reasonable because it can help us recognize from the perspective of the single frequency point that the IW will take place as long as the effective parameters valued at a certain frequency point meet the supporting conditions (A1 or A2), regardless of the actual property of the frequency dependency. In fact, the previous case (single-negative effective shear modulus) is also discussed in this way. Apart from that, a class of typical frequency dependency of the effective density is considered incidentally in the numerical example.

It can be found from the above analyses that the SH IW may exist as long as the effective shear modulus of the EMM half-space is negative, regardless of whether the effective density is positive or negative. However, this is specific to the joined half-spaces built from an EMM half-space and a normal one. Actually, for the more general case composed of two EMM half-spaces, the dispersion equation (4) still holds. Thus, there will exist two other combinations of effective parameters supporting the occurrence of the SH IW.

(1) One half-space is composed of an EMM medium with single-negative effective density while the other one has single-negative effective shear modulus;
(2) One with single-negative effective density while the other is double-negative.

We will discuss these two cases briefly in Sec. III B.

B. Joined half-spaces composed of two types of EMM

Figure 5 shows a schematic of the joined half-spaces composed of two types of EMM. The terms ρ_{m1} and μ_{m1} represent the effective density and effective shear modulus of the upper half-space and ρ_{m2} and μ_{m2} represent the effective density and effective shear modulus of the lower half-space, respectively. Similar to Eq. (1), the displacement fields of the SH wave in the respective half-spaces can be expressed as

$$
\begin{aligned}
u_3^{m1} &= C_1 e^{jpx_2} e^{j(kx_1 - \omega t)}, \\
u_3^{m2} &= C_2 e^{jqx_2} e^{j(kx_1 - \omega t)},
\end{aligned} \tag{5}
$$

where $p = \sqrt{\frac{\omega^2}{c_{m1}^2} - k^2}$, $c_{m1}^2 = \frac{\mu_{m1}}{\rho_{m1}}$, $q = \sqrt{\frac{\omega^2}{c_{m2}^2} - k^2}$, and $c_{m2}^2 = \frac{\mu_{m2}}{\rho_{m2}}$. Terms p and q still represent the wavenumbers in the upper and lower half-spaces, respectively, in the ρ_m, μ_m direction. A dispersion relation similar to Eq. (3) is obtained again according to the continuity requirement of shearing stress, namely,

$$
\mu_{m1}p = \mu_{m2}q. \tag{6}
$$

(1) Single-negative effective shear modulus and single-negative effective density

In this case, the upper and lower half-spaces are assumed to have single-negative effective shear modulus and single-effective density, respectively, namely, $\rho_{m1} > 0$,
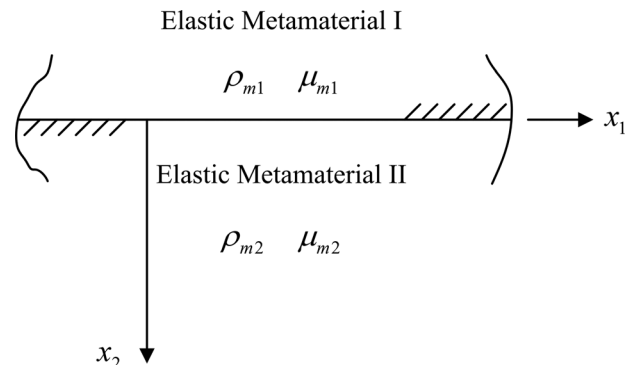
FIG. 5. Joined half-spaces composed of two types of EMM.

$\mu_{m1} < 0$, $\rho_{m2} < 0$, and $\mu_{m2} > 0$. Likewise, when considering the IW solution, p and q should take positive and negative imaginary numbers, respectively (similarly, $p = jp^*$ and $q = -jq^*$ are introduced, where $p^* = \sqrt{k^2 - \frac{\omega^2}{c_{m1}^2}}$, $q^* = \sqrt{k^2 - \frac{\omega^2}{c_{m2}^2}}$, and j is the imaginary unit). After introducing the effective-parameter ratios, namely, $a = \frac{-\rho_{m2}}{\rho_{m1}}$ and $b = \frac{-\mu_{m1}}{\mu_{m2}}$ ($a > 0, b > 0$), the dispersion relation of the IW can be derived from Eq. (6) as $k = \sqrt{\frac{a-b}{b^2-1}}\sqrt{\frac{\rho_{m1}}{\mu_{m2}}}\,\omega$. Correspondingly, the following two existence conditions supporting the (traveling) IW mode are obtained:

$$\text{Condition B1} : 1 < b < a.$$

$$\text{Condition B2} : 0 < a < b < 1.$$

For numerical illustration, two sets of parameters satisfying the above two conditions (respectively, $a = 8$, $b = 1.01$, 2, 3.5, 5.2, 7, and 7.99 and $a = 0.1$, $b = 0.101$, 0.18, 0.4, 0.7, 0.93, and 0.999) are selected arbitrarily, and the other parameters are assumed as $\rho_{m1} = 2600 \text{ kg/m}^3$ and $\mu_{m2} = 9 \text{ MPa}$. The calculated dispersion curves are depicted in Fig. 6.

Figure 6(a) shows the dispersion curves under condition B1. Clearly the curves approach the vertical axis as b tends to a. In fact, the transverse wave velocities of the upper and lower half-spaces tend to the same value as b tends to a (i.e., $c_{m1} \to c_{m2}$). Thus, $p = \sqrt{\frac{\omega^2}{c_{m1}^2} - k^2}$ and $q = \sqrt{\frac{\omega^2}{c_{m2}^2} - k^2}$ will also tend to the same value. Considering further the continuity requirement of the shearing stress on the interface [Eq. (6)], p and q will approach zero simultaneously in this limiting case. As can be observed from the displacement solution Eq. (5), this situation represents the upper and lower half-spaces fluctuating simultaneously as a whole along the x_1 direction (i.e., a bulk transverse wave). However, because there is a single-negative effective parameter in each half-space, the fluctuation cannot propagate effectively because its wavenumber is imaginary, that is, the real part of the wavenumber becomes zero. Hence,

the mode curve of the limiting case is represented by the y axis in Fig. 6(a). As in Sec. III A, the wavenumber k (in the x_1 direction) of the IW mode also increases gradually to infinity for a given frequency as b tends to unity, with the displacement field being confined to an ever-narrower region on either side of the interface. The dispersion curves under condition B2 are shown in Fig. 6(b), where the main behaviors of the IW modes are basically the same; we will not go into much detail about the properties of these curves.

In addition, there is also an edge case ($b = a = 1$) just as that mentioned in Sec. III A. Under this circumstance, the effective densities and effective shear moduli of the upper and lower half-paces are exactly opposite. The dispersion equation or the stress continuity relation on the interface becomes an identity and is independent of the wave frequency. In other words, a SH IW mode with an arbitrary real wavenumber k may possibly appear with any frequency in the vicinity of the interface.

(2) Double-negative effective parameters and single-negative effective density

For this case, the upper and lower half-spaces are assumed to be composed of one double-negative and one single-negative EMM medium, respectively, i.e., $\rho_{m1} < 0$, $\mu_{m1} < 0$, $\rho_{m2} < 0$, and $\mu_{m2} > 0$. Introducing the ratios $a = \frac{\rho_{m2}}{\rho_{m1}}$ and $b = \frac{-\mu_{m2}}{\mu_{m1}}$ ($a > 0, b > 0$) into Eq. (6), we have $k = \sqrt{\frac{ab+1}{1-b^2}}\sqrt{\frac{\rho_{m1}}{\mu_{m1}}}\,\omega$. Obviously, the condition $0 < b < 1$ is the only requirement for supporting the propagation of the expected SH IW.

We also choose a set of parameters for the numerical illustration, where $b = 0.2$, 0.8, 0.94, 0.97, 0.99, and 0.999, $\rho_{m1} = -2600 \text{ kg/m}^3$, $\mu_{m1} = -9 \text{ MPa}$, and $a = 2$. The calculated dispersion curves are shown in Fig. 7.

It can be seen that the SH IW mode tends to the bulk transverse wave mode of the upper half-space (namely, $\omega = kc_{m1}$, as denoted by the black dashed line in Fig. 7) as b tends to zero. This phenomenon is easily understood by recognizing that the bulk transverse wave velocity in the lower
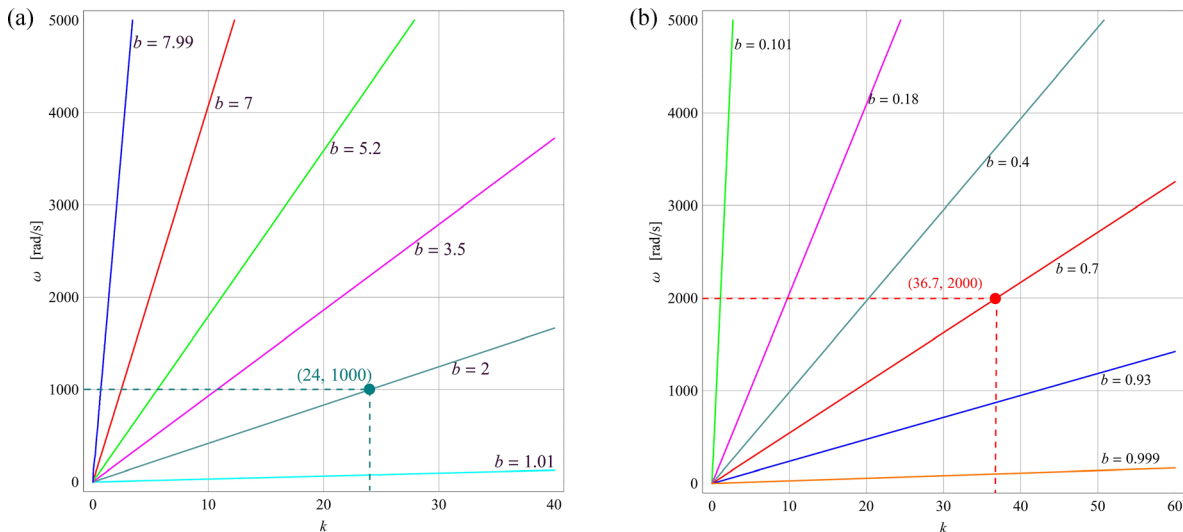

FIG. 6. SH IW modes in joined half-spaces composed of two types of EMM with $\rho_{m1} > 0$, $\mu_{m1} < 0$, $\rho_{m2} < 0$, and $\mu_{m2} > 0$. $\rho_{m1} = 2600 \text{ kg/m}^3$ and $\mu_{m2} = 9 \text{ MPa}$ are used in the calculations. (a) $a = 8$, $b = 1.01$, 2, 3.5, 5.2, 7, 7.99, corresponding to condition B1 and (b) $a = 0.1$, $b = 0.101$, 0.18, 0.4, 0.7, 0.93, 0.999, corresponding to condition B2.
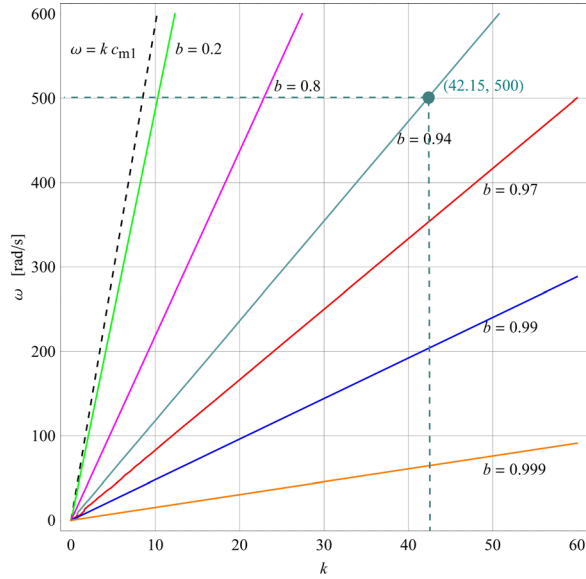
FIG. 7. SH IW modes in joined half-spaces composed of two types of EMM with $\rho_{m1} < 0$, $\mu_{m1} < 0$, $\rho_{m2} < 0$, and $\mu_{m2} > 0$. b = 0.2, 0.8, 0.94, 0.97, 0.99, and 0.999, $\rho_{m1} = -2600$ kg/m³, $\mu_{m1} = -9$ MPa, and $a = 2$ are used in the calculation.

half-space approaches zero as b tends to zero, i.e., $c_{m2} = \sqrt{\frac{\mu_{m2}}{\rho_{m2}}} = \sqrt{\frac{-b\,\mu_{m1}}{a\,\rho_{m1}}} \rightarrow 0$, meaning that the lower half-space tends to be composed of a fluid-like effective medium in this situation. As b tends to unity, the features of the wave modes are the same as those described before, namely that the wavenumber k (in the x_1 direction) of the IW increases gradually to infinity for a given frequency and the displacement field becomes confined into an ever-narrower region on either side of the interface.

According to the above discussion, all four possible combinations of the effective-medium parameters that support the SH IW mode in joined half-spaces built from EMMs are summarized and listed in Table I, together with the corresponding existence condition(s).

IV. FINITE-ELEMENT SIMULATIONS AND DEMONSTRATIONS

A. Simulation from the level of the effective medium

We conducted finite-element simulation with the effective-medium model by using the software COMSOL

TABLE I. Possible combinations of effective parameters supporting the SH IW mode, with the corresponding existence condition(s).

Effective parameter property of half-space 1	Effective parameter property of half-space 2	Existence condition 1	Existence condition 2
$\rho_1 > 0, \mu_1 < 0$	$\rho_2 > 0, \mu_2 > 0$	$0 < \frac{|\mu_1|}{\mu_2} < 1$	/
$\rho_1 < 0, \mu_1 < 0$	$\rho_2 > 0, \mu_2 > 0$	$0 < \frac{|\rho_1|}{\rho_2} < \frac{|\mu_1|}{\mu_2} < 1$	$1 < \frac{|\mu_1|}{\mu_2} < \frac{|\rho_1|}{\rho_2}$
$\rho_1 > 0, \mu_1 < 0$	$\rho_2 < 0, \mu_2 > 0$	$1 < \frac{|\mu_1|}{\mu_2} < \frac{|\rho_2|}{\rho_1}$	$0 < \frac{|\rho_2|}{\rho_1} < \frac{|\mu_1|}{\mu_2} < 1$
$\rho_1 < 0, \mu_1 < 0$	$\rho_2 < 0, \mu_2 > 0$	$0 < \frac{\mu_2}{|\mu_1|} < 1$	/

Multiphysics 5.0. The model settings and structural parameters are shown in Fig. 8, where several perfect matched layers are set at the upper, left-hand, and right-hand boundaries to prevent wave reflection. The lower boundary in the figure is specified as a symmetric boundary, while the continuity boundary constraint is applied to the front and back boundaries (see the side view in the right-hand panel). A harmonic edge load is exerted in the direction perpendicular to the $x_1 - x_2$ plane at the interface. Noting that the SH IW dispersion relation in Eq. (4) is related only to density and shear modulus, the Poisson's ratios of the materials are set to 0.3 by default during the simulation. The joined half-spaces composed of an EMM and a normal medium are simulated as follows:

(1) Case 1: double-positive parameters

First, the out-of-plane displacement-field distribution is computed for the case in which the EMM half-space has a simultaneously positive effective density and shear modulus. The medium parameters selected for simulation are listed in Table II (case 1), and the obtained wave field is shown in Fig. 9(a). Both half-spaces have real values of bulk transverse wave velocity in this case, as evidenced by the bulk wave effect. However, just as expected from the theoretical analysis, no SH IW appears.

(2) Case 2: single-negative effective density

The out-of-plane displacement-field distribution is calculated with the set of parameters listed in Table II (case 2) for which the EMM medium exhibits the property of single-negative effective density. As shown in Fig. 9(b), no SH IW can be found but the bulk wave. The observed bulk wave travels only in the normal half-space while being attenuated significantly in the EMM half-space because of the imaginary transverse wave velocity induced by the single-negative density property. It can be seen that the simulation results in this case and the previous one are consistent with the theoretical predictions given before.

(3) Case 3: single-negative effective shear modulus

For this case, a set of parameters is also specified as listed in Table II (case 3), and the computed out-of-plane displacement-field distribution is shown in Fig. 10(a). Evidently, a distinct SH IW appears in the vicinity of the interface formed by the two half-spaces, and the wave field is concentrated in a rather narrow region on either side of the interface. Furthermore, Fig. 10(b) gives the wave profile, from which the wavelength is estimated to be around 0.158 m after data extraction and processing. According to the analysis frequency of 57.3 Hz used here, we have marked the corresponding theoretical result on the dispersion curve, namely, the marked point (39.8, 0.6) (see the pink dot in Fig. 3, where the dimensionless frequency is 0.6, i.e., $f = \frac{\omega}{2\pi} = \frac{0.6\omega_0}{2\pi} = \frac{0.6 \times 600}{2\pi} = 57.3$ Hz). Clearly, the simulation result here agrees well with the theoretical prediction ($\lambda = \frac{2\pi}{k} = \frac{2\pi}{39.8} = 0.158$ m).

Rather than a bulk wave field, a SH IW appears in Fig. 10(a). In fact, the bulk wave still exists on the side of the normal half-space, although it is not obvious because of the
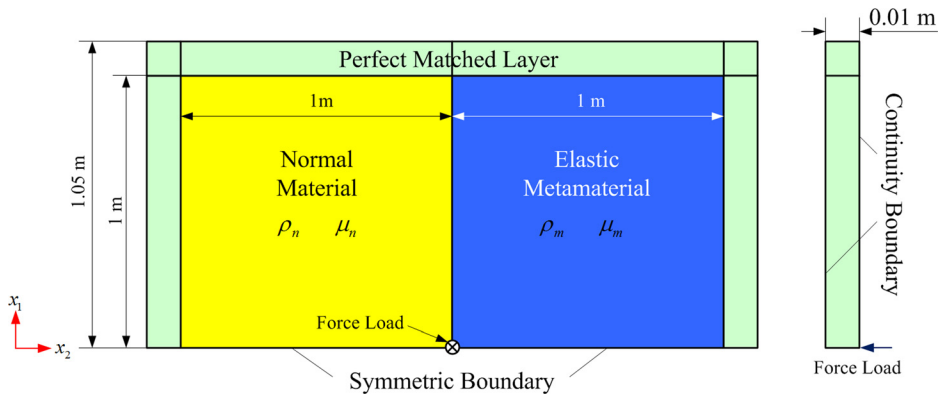
FIG. 8. Simulation model of joined half-spaces composed of EMM and normal medium.

TABLE II. Simulation parameters of joined half-spaces composed of EMM and normal medium.

EMM effective-parameter property	ρ_n (kg/m^3)	ρ_m (kg/m^3)	μ_n (MPa)	μ_m (MPa)	f (Hz)
Case 1: double-positive parameters	2600	5200	9	7.2	100
Case 2: single-negative effective density	2600	−5200	9	7.2	57.3
Case 3: single-negative effective shear modulus	2600	3926.12	9	−8.73	57.3
Case 4: double-negative parameters (Condition A1)	2600	−1170	9	−8.1	159.15
Case 5: double-negative parameters (Condition A2)	2600	−7800	9	−11.7	159.15

strong intensity of the IW. For illustration, we extract the out-of-plane displacement distribution from a hypothetical line that is perpendicular to the interface in the middle part of the model [i.e., the horizontal line AG in Fig. 10(a)]. The
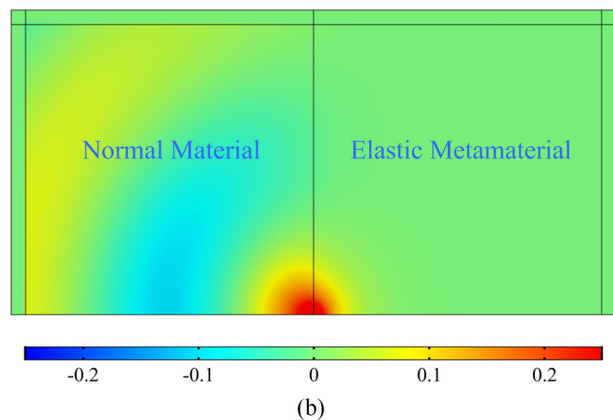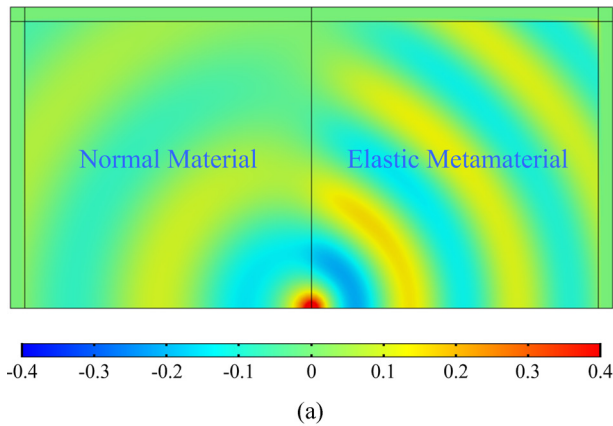

(a)

(b)

FIG. 9. Displacement-field distributions of joined half-spaces composed of a normal medium and an EMM with (a) double-positive parameters and (b) single-negative effective density.

results of doing so are shown in Fig. 10(c), the ordinate of which represents the ratio of (i) the out-of-plane displacement calculated by simulation to (ii) the prescribed displacement at the loading edge. In Fig. 10(c), the out-of-plane displacement distribution on the interface can be seen easily, and a relatively weak bulk wave traveling in the normal side can be found. Meanwhile, rather than a traveling bulk wave, an evanescent one appears in the EMM side because of the imaginary bulk transverse wave velocity. It is worth noting in passing that the IW intensity is much stronger than the concurrent bulk wave. This is obviously unfavorable for applications of SH-wave isolation and related object protection (e.g., in the field of seismic waves) despite the fact that the propagation of the bulk transverse wave could be suppressed effectively by using EMMs with single-negative parameters. It would be interesting and meaningful to further investigate the wave-energy allocation ratio between the bulk wave mode and the IW mode under general forced excitation. However, that goes beyond the scope of this paper and will be discussed elsewhere.

(4) Cases 4 and 5: double-negative parameters

The wave field corresponding to two sets of effective parameters that respectively satisfy the two supporting conditions (namely A1 and A2) are obtained as shown in Figs. 11(a)–11(c) and 11(d)–11(f), respectively. The medium parameters used in the simulations are given in Table II (see cases 4 and 5), and the analysis frequency is 159.15 Hz (corresponding to an angular frequency of 1000 rad/s). Similarly, the related theoretical results are marked in Figs. 4(a) and 4(b) [i.e., the points (30.12, 1000) and (34.75, 1000), respectively].

There are distinct bulk waves traveling in both half-spaces for the double-negative effective parameters, while a significant traveling SH wave appears in the vicinity of the interface. For case 4 ($a = 0.45$ and $b = 0.9$, corresponding to condition A1), the wavelength of the IW is obtained as
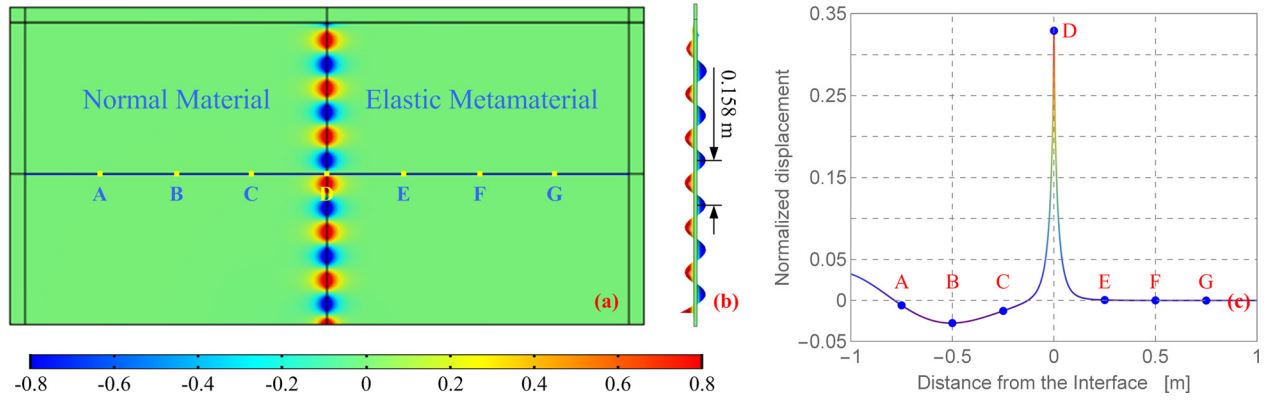
FIG. 10. Displacement field of the SH wave in joined half-spaces composed of a normal medium and an EMM with single-negative effective shear modulus.
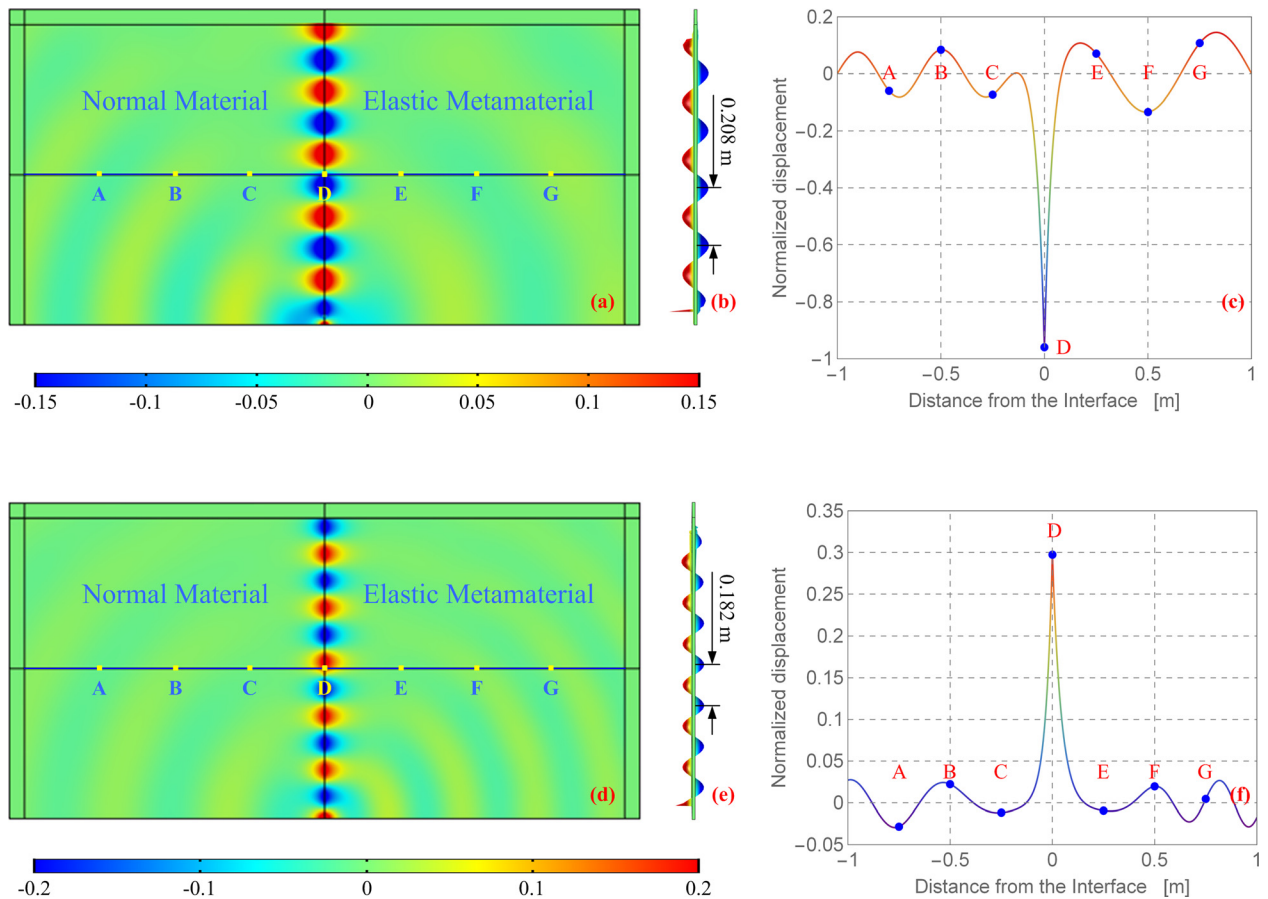

FIG. 11. Displacement field of the SH wave in joined half-spaces composed of a normal medium and an EMM with double-negative parameters: (a)–(c) corresponding to condition A1, $a = 0.45$, and $b = 0.9$; (d)–(f) corresponding to condition A2, $a = 3$, and $b = 1.3$.

0.208 m [as shown in Figs. 11(a)–11(c)], while the theoretical result is $\lambda = \frac{2\pi}{k} = \frac{2\pi}{30.12} = 0.209$ m. For case 5 ($a = 3$ and $b = 1.3$, corresponding to condition A2), the wavelength calculated from the wave-field data is around 0.182 m [as shown in Figs. 11(d)–11(f)], while the theoretical value is $\lambda = \frac{2\pi}{k} = \frac{2\pi}{34.75} = 0.181$ m. Obviously, these results agree well.

(5) Cases 6 and 7: single-negative effective shear modulus and single-negative effective density.

    We use the same finite-element model to simulate the joined half-spaces built from two types of EMM. For the

situation in which one of the EMMs has a single-negative effective shear modulus while the other possesses a single-negative effective density, two cases (conditions B1 and B2) are considered here; the medium parameters are given in Table III (cases 6 and 7). For comparison, the analysis frequencies are selected here as 159.15 Hz and 318.31 Hz, respectively, and the theoretical results are marked in Fig. 6 [i.e., the points (24, 1000) and (36.7, 2000), respectively]. Figures 12(a)–12(c) and 12(d)–12(f) exhibit the out-of-plane displacement-field distributions of these two cases, respectively. There is no bulk wave in either half-space because of

TABLE III. Simulation parameters of joined half-spaces with two types of EMM.

EMM effective-medium property combination	ρ_{m1} (kg/m³)	ρ_{m2} (kg/m³)	μ_{m1} (MPa)	μ_{m2} (MPa)	f (Hz)
Case 6: single-negative effective shear modulus/single-negative effective density (condition B1)	2600	−20 800	−18	9	159.15
Case 7: single-negative effective shear modulus/single-negative effective density (Condition B2)	2600	−260	−6.3	9	318.31
Case 8: single-negative effective density/double- negative parameters	−2600	−5200	−9	8.46	79.58

the imaginary bulk transverse wave velocities induced by the single-negative property. However, the SH IW can be observed clearly near the interface just as predicted by the theoretical analysis given before. If we check the wavelengths according to the simulation results (0.263 m and 0.172 m for cases 6 and 7, respectively), a good agreement is again found with the theoretical values.

(6) Case 8: single-negative effective density/double-negative effective parameters.

Figure 13 shows the wave field when one EMM medium has single-negative effective density while the other has double-negative effective parameters; the medium parameters are given in Table III (case 8). It is natural that the bulk wave appears only in the EMM half-space with double-negative parameters (the left-hand side) because of the real value of the effective bulk transverse wave velocity, while evanescent waves occur in the other side because of the imaginary wave velocity induced by the single-negative

density. Apart from the bulk wave field, a distinct SH IW is found traveling in the vicinity of the interface once again with a much stronger intensity than that of the bulk wave field. The wavelength calculated from the simulation is around 0.149 m, which is also consistent with the theoretical result (refer to the marked point (42.15, 500) in Fig. 7).

B. Simulation from the level of the microstructural unit cell

To verify the theoretical results with practical materials, an appropriate three-dimensional EMM unit cell is presented and analyzed in this subsection. The unit cell is composed of a three-component continuous medium comprising a silicon-rubber-coated epoxy sphere embedded in a polyethylene foam matrix in a SC (simple cubic) lattice, as shown in Fig. 14(a). The radius of the epoxy sphere is 4.2 mm, the thickness of the rubber coating is 5.4 mm, and the length of the cube edge is 30 mm (hence the filling fraction is around
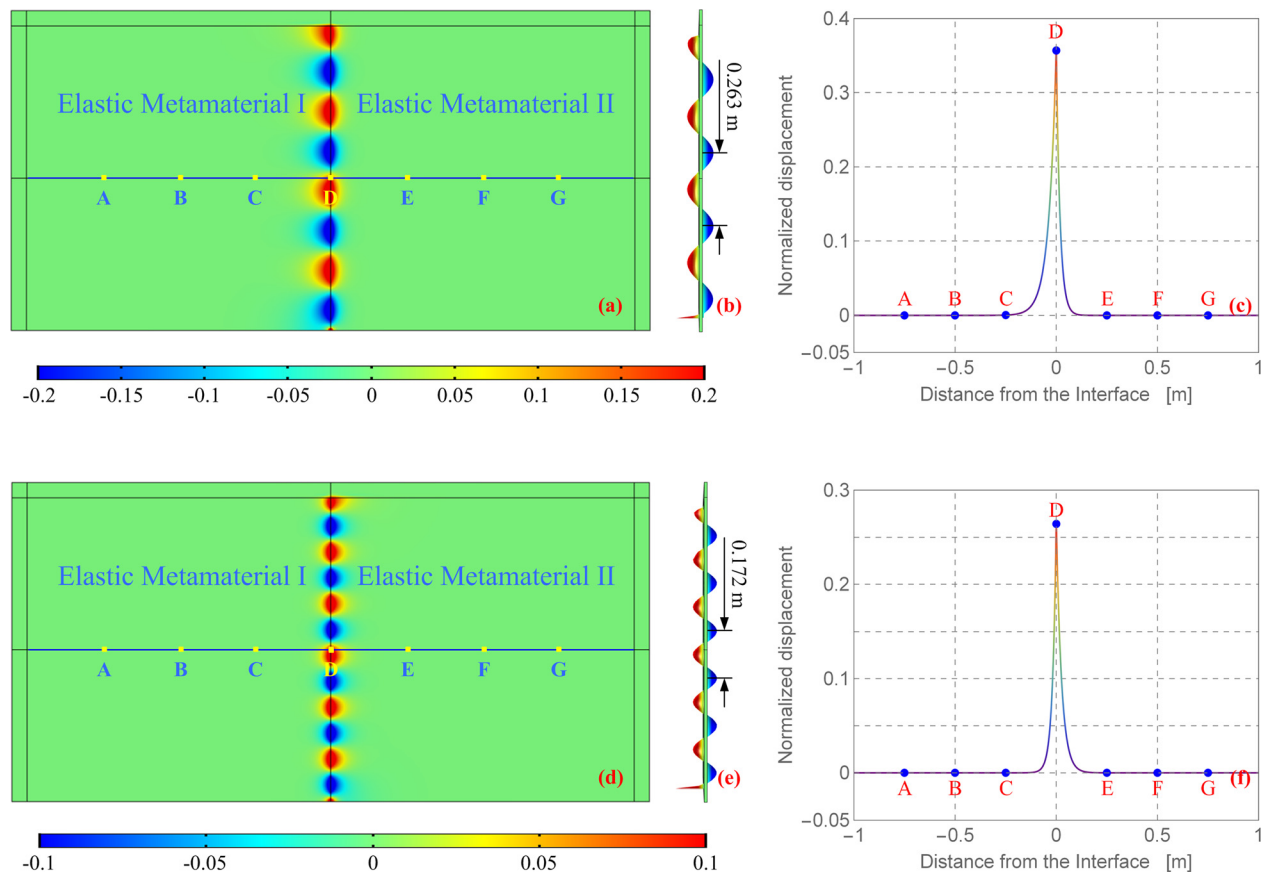

FIG. 12. Displacement field of the SH wave in joined half-spaces composed of two types of EMM, one with single-negative effective shear modulus and the other with single-negative effective density: (a)–(c) corresponding to condition B1, $a = 8$, and $b = 2$; (d)–(f) corresponding to condition B2, $a = 0.1$, and $b = 0.7$.
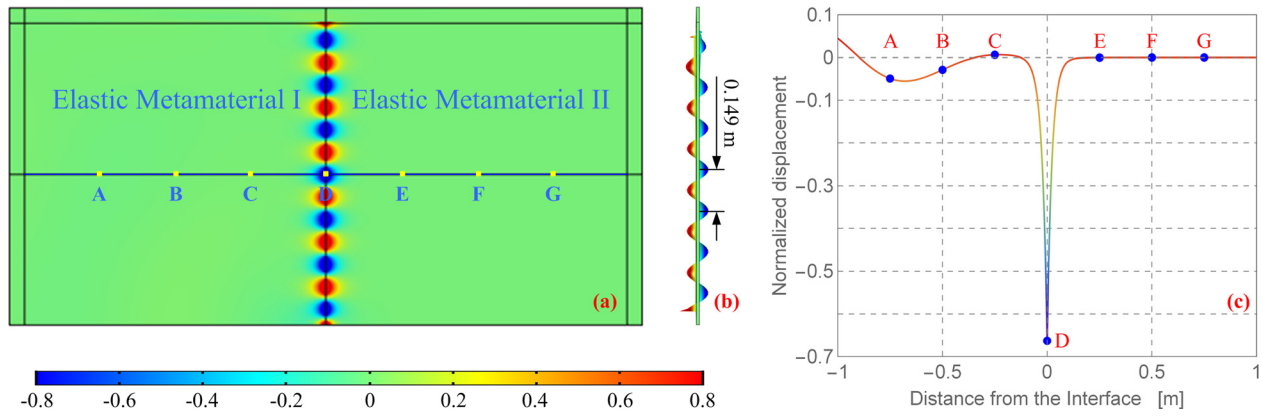
FIG. 13. Displacement field of the SH wave in joined half-spaces composed of two types of EMM, one with single-negative effective density and the other with double-negative parameters.

13.7%). The material parameters (mass density and Lamé constants) are as follows: polyethylene foam, $\rho_P = 115$ kg/m^3, $\lambda_P = 6$ MPa, and $\mu_P = 3$ MPa; silicon rubber, $\rho_S = 1300$ kg/m^3, $\lambda_S = 0.6$ MPa, and $\mu_S = 0.04$ MPa; epoxy, $\rho_E = 1180$ kg/m^3, $\lambda_E = 4430$ MPa, and $\mu_E = 1590$ MPa.

The effective mass density, bulk modulus, and shear modulus of the EMM built with the unit cell are calculated by using the "feel and response" method proposed in Refs. 33–35. Their frequency response curves (normalized to the corresponding medium parameter of the matrix) are shown in Fig. 14(b), where the symbol a is the lattice constant

(30 mm) and $\tilde{c}$ is the S wave velocity of the polyethylene foam (matrix). It can be seen that within two ranges of dimensionless frequency, namely 0.1050–0.1078 and 0.1385–0.1793, the effective density is negative (because of the internal dipole resonance of the unit cell), while both of the effective moduli are positive, implying that bulk longitudinal and transverse waves cannot propagate in these two frequency bands. Besides, there exists another frequency range (0.1905–0.2007) in which only the effective shear modulus takes negative values (induced by the internal quadrupole resonance of the unit cell). Within this frequency
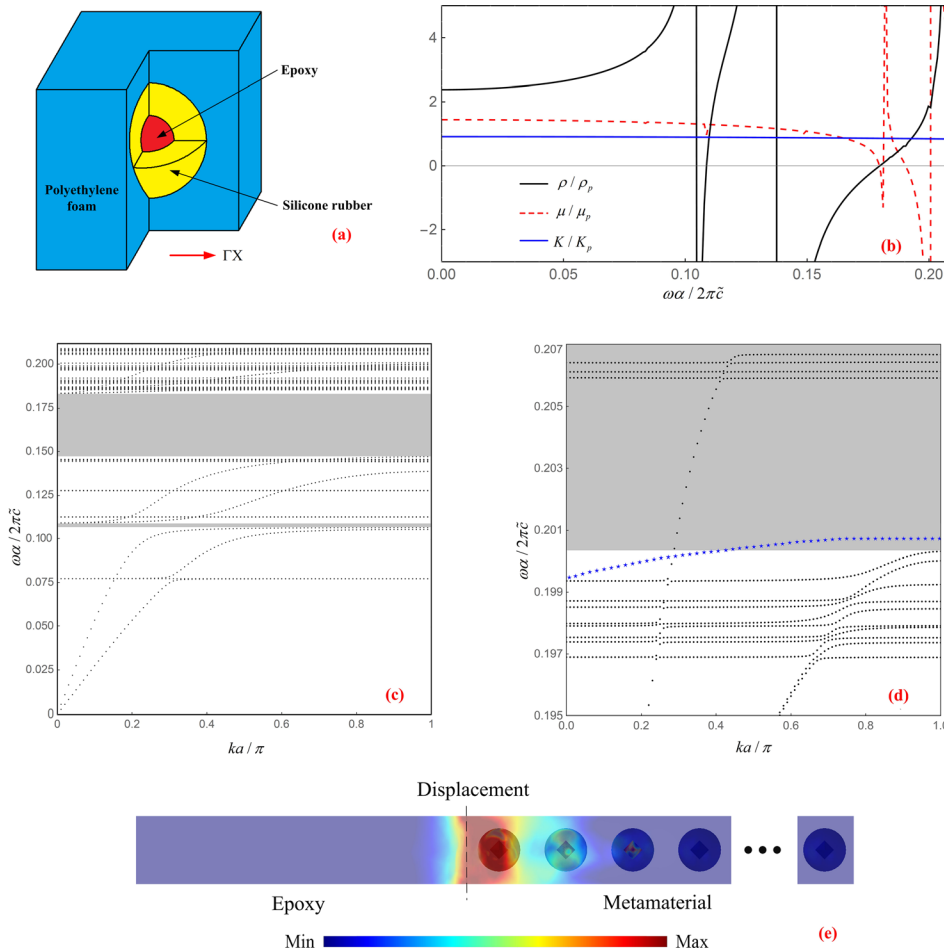

FIG. 14. (a) EMM unit cell. (b) EMM effective parameters computed by the "feel and response" method. (c) Band structure along the ΓX direction for the SC lattice built by the unit cell in (a). (d) Dispersion curve of the SH wave mode near frequency corresponding to zero effective shear modulus (indicated by blue asterisks) computed with the super cell. (e) Field distribution of eigenstates of the SH IW mode with $ka/\pi = 0.75$.

range, the bulk transverse wave will be suppressed completely while the bulk longitudinal wave can still propagate within a limited frequency interval until the effective longitudinal modulus ($K + \frac{4\mu}{3}$) turns negative as well. The band structure along the ΓX direction for the SC lattice is presented in Fig. 14(c). The band gaps within the frequency ranges 0.1067–0.1094 and 0.1454–0.1834 are fairly consistent with the results of the effective parameters. The band structure also shows that the effective shear modulus becomes negative within the range 0.1997–0.2072 in which the effective density and longitudinal modulus are both positive. The band structure in this frequency range is enlarged in Fig. 14(d) (the shaded area), from which we find that only the longitudinal wave mode exists while the transverse wave modes vanish, as predicted by the effective parameters.

To verify the SH IW mode in the joined half-spaces, we construct a super cell with 13 cells and an epoxy square bar [as shown in Fig. 14(e)]. The interface modes of this super cell are carried out by finite-element simulation, and the calculated SH IW dispersion curve is shown in Fig. 14(d) by the blue asterisks. Comparing with the band structure of the unit cell, we discover that the SH IW exists in the vicinity of the lower edge of the shaded area (single-negative effective shear modulus interval). Moreover, it should be noted that the lower edge corresponds to zero effective shear modulus of the EMM and, referring to the curves of the effective parameters [Fig. 14(b)], it is not difficult to understand that the narrow frequency interval is just the one that can satisfy the supporting condition of the SH IW discussed in case 3, i.e., $0 < b < 1$, where b was defined there as the (effective) shear modulus ratio between the component half-spaces ($b = \frac{-\mu_m}{\mu_n}$). Figure 14(e) shows the eigenstates for the SH IW mode with $ka/\pi = 0.75$, from which we further verify that the wave fields are confined strongly near to the interface.

It is worth pointing out that we have demonstrated only the case in which the joined half-spaces are composed of a normal medium and an EMM with single-negative effective shear modulus; the other three cases remain unverified (on the level of the microstructural unit cell). One reason is that the appropriate unit-cell structures are not easy to find because of the stricter requirements of the effective parameters, and another is that the frequency band in which the desired effective-medium properties could be even achieved is often too narrow for demonstration (and thus far there seems to be no general way to broaden it).

V. SUMMARY AND CONCLUSIONS

Unlike bulk-wave analysis in an unlimited domain, joined half-spaces have an interface, and it is well known that, as well as the original bulk-wave solutions, IW solutions may exist in the vicinity of this boundary. The main focus of interest in the present paper has been the problem of whether similar IWs can still exist when the joined half-spaces (either one or both) are built from EMMs.

Our research shows that a class of traveling SH IWs may exist in the vicinity of the interface under four specific combinations of effective-medium parameters. For the joined half-spaces composed of a normal medium and an

EMM, no such SH IW mode can exist if the EMM possesses double-positive effective parameters or single-negative effective density. However, such a wave mode may occur near the interface when the effective shear modulus of the EMM medium is negative, regardless of whether the effective density is positive or negative. The other two combinations appear in joined half-spaces composed of two types of EMM, namely (i) one half-space has single-negative effective density while the other has single-negative effective shear modulus and (ii) one half-space has double-negative effective parameters while the other has single-negative effective density. However, these four combinations of effective parameters provide only the possibility for a SH IW to occur. Corresponding existence conditions established in terms of effective-parameter ratios should be further satisfied to realize such wave modes.

According to the analysis results, we should pay special attention to this IW mode when considering the isolation, protection, or regulation of SH waves based on the EMM concept. Although a SH bulk wave can be blocked effectively by using the bulk-transverse-wave band gaps caused by single-negative parameters, these possible IWs can still occur under specific conditions (even including the condition of single-negative parameters) and should not be overlooked because they may have much more serious impacts on the protected objects (e.g., the foundations of a high-rise building). Similarly, we have been concerned only with SH waves, but it is inevitable that P and SV waves will exist in practical applications. Therefore, attention should also be paid to understanding and manipulating those waves based on EMM technology, something that we intend to do in future work.

[1]Z. Y. Liu, X. X. Zhang, Y. W. Mao, Y. Y. Zhu, Z. Y. Yang, C. T. Chan, and P. Sheng, "Locally resonant sonic materials," Science **289**, 1734–1736 (2000).

[2]Y. F. Wang, Y. S. Wang, and L. Wang, "Two-dimensional ternary locally resonant phononic crystals with a comblike coating," J. Phys. D: Appl. Phys. **47**(1), 015502 (2014).

[3]Y. Q. Liu, X. Y. Su, and C. T. Sun, "Broadband elastic metamaterial with single negativity by mimicking lattice systems," J. Mech. Phys. Solids **74**, 158–174 (2015).

[4]E. D. Nobrega, F. Gautier, A. Pelat, and J. M. C. Dos Santos, "Vibration band gaps for elastic metamaterial rods using wave finite element method," Mech. Syst. Signal Process. **79**, 192–202 (2016).

[5]Z. Yang, J. Mei, M. Yang *et al.*, "Membrane-type acoustic metamaterial with negative dynamic mass," Phys. Rev. Lett. **101**, 204301 (2008).

[6]M. Farhat, S. Guenneau, and S. Enoch, "Ultrabroadband elastic cloaking in thin plates," Phys. Rev. Lett. **103**, 024301 (2009).

[7]N. Stenger, M. Wilhelm, and M. Wegener, "Experiments on elastic cloaking in thin plates," Phys. Rev. Lett. **108**, 014301 (2012).

[8]R. Zhu, X. N. Liu, G. K. Hu, C. T. Sun, and G. L. Huang, "Negative refraction of elastic waves at the deep-subwavelength scale in a single-phase metamaterial," Nat. Commun. **5**, 5510 (2014).

[9]M. Dubois, M. Farhat, E. Bossy, S. Enoch, S. Guenneau, and P. Sebbah, "Flat lens for pulse focusing of elastic waves in thin plates," Appl. Phys. Lett. **103**, 071915 (2013).

[10]M. Dubois, E. Bossy, S. Enoch, S. Guenneau, G. Lerosey, and P. Sebbah, "Time-driven superoscillations with negative refraction," Phys. Rev. Lett. **114**, 013902 (2015).

[11]A. Colombi, P. Roux, and M. Rupin, "Sub-wavelength energy trapping of elastic waves in a metamaterial," J. Acoust. Soc. Am. **136**(2), 192–198 (2014).

[12]D. Bigoni, S. Guenneau, A. B. Movchan, and M. Brun, "Elastic metamaterials with inertial locally resonant structures: Application to lensing and localization," Phys. Rev. B: Condens. Matter **87**, 174303 (2013).

[13]R. Zhu, Y. Y. Chen, Y. S. Wang *et al.*, "A single-phase elastic hyperbolic metamaterial with anisotropic mass density," J. Acoust. Soc. Am. **139**(6), 3303 (2016).

[14]P. A. Deymier, *Acoustic Metamaterials and Phononic Crystals* (Springer-Verlag, Berlin, Heidelberg, 2013), pp. 201–205.

[15]G. Ma and P. Sheng, "Acoustic metamaterials: From local resonances to broad horizons," Sci. Adv. **2**, 1501595 (2016).

[16]N. Fang, D. J. Xi, J. Y. Xu, M. Ambati, W. Srituravanich, C. Sun, and X. Zhang, "Ultrasonic metamaterials with negative modulus," Nat. Mater. **5**, 452–456 (2006).

[17]M. Yang, G. Ma, Z. Yang, and P. Sheng, "Coupled membranes with doubly negative mass density and bulk modulus," Phys. Rev. Lett. **110**, 134301 (2013).

[18]C.-N. Weng, P.-W. Chang, and T. Chen, "Numerical simulation of broadband bi-negative elastic metamaterials and wave transmission properties," Procedia Eng. **79**, 622–630 (2014).

[19]Y. Ding, Z. Liu, C. Qiu, and J. Shi, "Metamaterial with simultaneously negative bulk modulus and mass density," Phys. Rev. Lett. **99**, 093904 (2007).

[20]Y. Wu, Y. Lai, and Z.-Q. Zhang, "Effective medium theories and symmetry properties of elastic metamaterials," in *Metamaterial*, edited by X.-Y. Jiang (InTech, 2012), pp. 143–168.

[21]Y. Wu, Y. Lai, and Z.-Q. Zhang, "Effective medium theory for elastic metamaterials in two dimensions," Phys. Rev. B **76**, 205313 (2007).

[22]R. Zhu, X. N. Liu, G. L. Huang, H. H. Huang, and C. T. Sun, "Microstructural design and experimental validation of elastic metamaterial plates with anisotropic mass density," Phys. Rev. B **86**, 144307 (2012).

[23]R. Zhu, X. N. Liu, and G. L. Huang, "Study of anomalous wave propagation and reflection in semi-infinite elastic metamaterials," Wave Motion **55**, 73–83 (2015).

[24]N. Kaina, F. Lemoult, M. Fink *et al.*, "Negative refractive index and acoustic superlens from multiple scattering in single negative metamaterials," Nature **525**, 77 (2015).

[25]X. Wang, "Dynamic behavior of a metamaterial system with negative mass and modulus," Int. J. Solids Struct. **51**, 1534–1541 (2014).

[26]O. J. Hwan, K. Y. Eui, L. H. Jin *et al.*, "Elastic metamaterials for independent realization of negativity in density and stiffness," Sci. Rep. **6**, 23630 (2016).

[27]H. H. Huang, C. T. Sun, and G. L. Huang, "On the negative effective mass density in acoustic metamaterials," Int. J. Eng. Sci. **47**, 610–617 (2009).

[28]Y. Wu, Y. Lai, and Z.-Q. Zhang, "Elastic metamaterials with simultaneously negative effective shear modulus and mass density," Phys. Rev. Lett. **107**, 105506 (2011).

[29]R. Zhu, X. N. Liu, G. K. Hu, F. G. Yuan, and G. L. Huang, "Microstructural designs of plate-type elastic metamaterial and their potential applications: A review," Int. J. Smart Nano Mater. **6**(1), 14–40 (2015).

[30]P. Sheng and B. van Tiggelen, "Introduction to Wave Scattering, Localization and Mesoscopic Phenomena. Second edition," Waves Random Complex Media **17**(2), 235–237 (2007).

[31]J. S. Li and C. T. Chan, "Double-negative acoustic metamaterial," Phys. Rev. E **70**, 055602 (2004).

[32]Y. F. Wang, Y. S. Wang, and V. Laude, "Wave propagation in two-dimensional viscoelastic metamaterials," Phys. Rev. B **92**, 104110 (2015).

[33]K. Deng, Y. Ding, Z. He, H. Zhao, J. Shi, and Z. Liu, "Theoretical study of subwavelength imaging by acoustic metamaterial slabs," J. Appl. Phys. **105**, 124909 (2009).

[34]Y. Lai, Y. Wu, P. Sheng, and Z. Q. Zhang, "Hybrid elastic solids," Nat. Mater. **10**, 620–624 (2011).

[35]X. N. Liu, G. K. Hu, G. L. Huang, and C. T. Sun, "An elastic metamaterial with simultaneously negative mass density and bulk modulus," Appl. Phys. Lett. **98**, 251907 (2011).

[36]Y. F. Wang, Y. S. Wang, and C. Zhang, "Two-dimensional locally resonant elastic metamaterials with chiral comb-like interlayers: Bandgap and simultaneously double negative properties," J. Acoust. Soc. Am. **139**, 3311–3319 (2016).

[37]H. W. Dong, S. D. Zhao, Y. S. Wang *et al.*, "Topology optimization of anisotropic broadband double-negative elastic metamaterials," J. Mech. Phys. Solids **105**, 54–80 (2017).

[38]S. J. Mitchell, A. Pandolfi, and M. Ortiz, "Metaconcrete: Designed aggregates to enhance dynamic performance," J. Mech. Phys. Solids **65**, 69–81 (2014).

[39]N. Aravantinos-Iafiris and M. M. Sigalas, "Large scale phononic metamaterials for seismic isolation," J. Appl. Phys. **118**, 064901 (2015).

[40]K. T. Tan, H. H. Huang, and C. T. Sun, "Blast-wave impact mitigation using negative effective mass density concept of elastic metamaterials," Int. J. Impact Eng. **64**, 20–29 (2014).

[41]S.-H. Kim and M. P. Das, "Artificial seismic shadow zone by acoustic metamaterials," Mod. Phys. Lett. B **27**(20), 1350140 (2013).

[42]A. A. Oliner, *Acoustic Surface Waves* (Springer-Verlag, Berlin, Heidelberg, New York, 1978).

[43]J. Achenbach, *Wave Propagation in Elastic Solids* (North-Holland Publishing Company, 1973).

[44]K. Deng, Z. He, Y. Ding, H. Zhao, and Z. Liu, "Surface-plasmon-polariton (SPP)-like acoustic surface waves on elastic metamaterials," e-print arXiv:1408.2186v1.